Sound velocity of α-quartz under pressure: First-principles calculations

Zhi-Xin Bai [1,*] Xin Qu,[1] Cheng-Lu Jiang,[2] Zheng-Tang Liu,[3] and Qi-Jun Liu[1,4,†]

[1]*Bond and Band Engineering Group, School of Physical Science and Technology, Southwest Jiaotong University, Chengdu 610031, People's Republic of China*

[2]*College of Water Conservancy and Hydropower Engineering, Sichuan Agricultural University, Ya' an 625014, People's Republic of China*

[3]*State Key Laboratory of Solidification Processing, Northwestern Polytechnical University, Xi'an 710072, People's Republic of China*

[4]*College of Physics, Chongqing University, Chongqing 400044, People's Republic of China*

As the most abundant substance on the earth's crust, the behavior of α-quartz under pressure has always been a research hotspot, which has inherent crystallographic significance and is of significance to understanding the rocky parts of the earth. This paper provides the discussion about the stability of α-quartz under pressure by analyzing its sound velocity based on first-principles calculation. It is discovered that under pressure, the mechanical instability (24.5 GPa) of α-quartz precedes the dynamic instability (40 GPa). The results show that the trend of increasing and then decreasing for compressed sound velocity in different directions occurs before the structural change, and the pressure point that starts to decrease is about 20 GPa. The mechanical instability at 24.5 GPa is caused by amorphization of α-quartz. The propagation velocities of the plastic wave in crystal after structural change under pressure are discussed. It is considered that the plastic wave first propagates along the direction *K* to *G* in the *a* axis, and the velocity is about 429 m/s.

I. INTRODUCTION

Silica, exhibiting a very rich diversity of polymorphisms, with more than 30 stable or metastable forms, is a very abundant component in the earth [1]. Because of its abundance in nature, high-pressure phase transitions in silica have long been of great interest in the fields of geophysics, materials science, and condensed matter physics [2–10]. At lower pressures, Si forms tetrahedral coordination with O in silicon polymorphs, such as quartz [11], cristobalite [12], tridymite [13], and coesite [14]. When the pressure is approximately above 10 GPa, the coordination number of Si increases from 4 to 6, such as rutile type (stishovite) [15], CaCl$_2$ type [16], α-PbO$_2$ type (seifertite) [17], FeS$_2$ (pyrite) type [18], Fe$_2$P type [18], etc. Furthermore, metastable high-pressure structures of silica have also attracted extensive attention due to their exotic properties [19–25]. α-quartz, the most common and stable quartz crystal at ambient temperature and pressure, is not only an important part of quartz and silicate, but also the most abundant material on the earth. Studying its high-pressure behavior is not only because of its inherent crystallographic significance, but also because it has important implications for understanding the rocky portion of the earth. Hence, the behavior of α-quartz under pressure has been intensively studied up to now.

In 1988, Hemley *et al.* [26] made a meaningful experiment of pressure-induced amorphous phenomena in α-quartz at 25–30 GPa and 300 K. Thereafter, this discovery of pressure-induced amorphous phenomena in α-quartz has aroused great

interest. Tse and Klug [27] concluded that the mechanical instability at 22.3 GPa results in amorphous phenomena in α-quartz based on the constant-pressure molecular dynamics calculations. Binggeli and Chelikowsky [28], using a classical interatomic potential and a first-principles pseudopotential method, reported a mechanical instability in α-quartz at approximately 30 GPa, and believed that pressure-induced amorphization is due to shear instability. Kingma *et al.* [29] observed microscopically that the amorphization in α-quartz began with defect formation, followed by the growth of amorphous silicon dioxide in these defect sites.

Instead, in 1993, it was found experimentally by Kingma *et al.* [30] that the α-quartz undergoes a different crystalline-crystalline phase transition at 21 GPa and room temperature, followed by the amorphization of different crystal phases under pressure. Similarly, Binggeli *et al.* [31] found that α-quartz undergoes a phase transition (at 21.5 GPa) within the pressure range of amorphization using extensive molecular-dynamics simulations. Remarkably, in 1996, Kingma *et al.* [32] revealed experimentally the coexistence of at least one amorphization and two crystalline phases (quartz-II and a high-pressure phase) from 21 to 43 GPa. Moreover, a triclinic crystalline structure (at 22 GPa) had been found between α-quartz and the amorphous phase based on the classical molecular-dynamics calculations by Tse *et al.* [33]. It has also been shown experimentally by Haines *et al.* [1] that pressurizing α-quartz to 45 GPa produces a different monoclinic crystalline phase.

Based on the above research results, it can be found that although considerable work has been carried out to elucidate the structural evolution of α-quartz under pressure, further research in both experimental and theoretical aspects is still necessary to clarify the stability of α-quartz under pressure.

*Corresponding author: bai@my.swjtu.edu.cn

†Corresponding author: qijunliu@home.swjtu.edu.cn

144105-1

This therefore motivated us to further explore its stability under pressure. The solid material has the characteristic of force deformation, including elastic deformation and plastic deformation. Under the action of pressure, the propagation behavior of the elastic wave of lattice vibration before structural changes is generally characterized by the sound velocity. The average sound velocity (v_m) refers to the propagation speed of the elastic wave in the whole crystal, and the longitudinal and transverse wave sound velocities (v_l and v_t) represent the propagation speed of the elastic wave in the longitudinal and transverse directions of the crystal, respectively. They can be simply obtained from the bulk modulus (B), shear modulus (G), and lattice density (ρ). The compressed sound velocity (v_p) can describe the propagation direction of the elastic wave more specifically than v_m, which is related to phonon energy and momentum space. When the stress in the material exceeds the elastic limit, the plastic deformation will occur, that is, the change in the crystal structure. The effect of the generation of plastic deformation and its propagation in the crystal on the structural phase transition of materials is of vital importance. In summary, the propagation of sound velocity in the lattice plays an important role in the study of material stability.

Therefore, this paper aims to describe the stability of α-quartz under pressure by analyzing the change of sound velocity. Moreover, it is generally believed that phonon calculations can provide a standard for dynamic stability and indicate structural stability by the absence of virtual phonon frequencies [34,35]. In this paper, we draw lessons from the formula for calculating the compressional sound velocity (v_p), assuming that the velocity derived from the energy of the acoustic phonon imaginary frequency can be used to describe propagation velocity of plastic wave and denoted as v_q.

II. COMPUTATIONAL METHODS AND DETAILS

A. Computational methods

1. Sound velocity

The average sound velocity (v_m) can be obtained from bulk modulus (B), shear modulus (G), and density (ρ), expressed as follows [36]:

$$v_m = \left[\frac{1}{3}\left(\frac{2}{v_t^3} + \frac{1}{v_l^3}\right)\right]^{-1/3}, \qquad (1)$$

$$v_l = \left(\frac{3B + 4G}{3\rho}\right)^{1/2}, \qquad (2)$$

$$v_t = \left(\frac{G}{\rho}\right)^{1/2}, \qquad (3)$$

where v_l is the longitudinal wave velocity, and v_t is the transverse wave velocity. The computational details of B and G are described in Supplemental Material (SM) Sec. I [37].

The compressional sound velocity (v_p) is determined by fitting the phonon dispersion with a sinusoidal function, and the calculated formula is as follows [47]:

$$E = 4.192 \times 10^{-4} v_p \times Q_{\max} \sin\left(\frac{\pi}{2}\frac{Q}{Q_{\max}}\right), \qquad (4)$$

where, E (meV) and Q (nm^{-1}) are the energy and the momentum of the acoustic phonon, and $Q_{\max}$ (nm^{-1}) is the length of
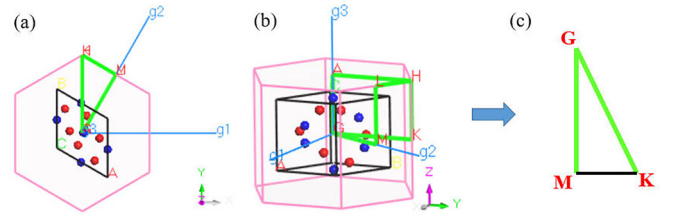

FIG. 1. (a),(b) The view of Brillouin zone of α-quartz unit cell from different perspectives, the $\overrightarrow{g_1}$, $\overrightarrow{g_2}$, and $\overrightarrow{g_3}$ are reciprocal lattice vector; (c) the geometric diagram of K-point G (0 0 0), K (-0.333 0.667 0) and M (0, 0.5 0), $\angle MGK = 30°$, $\angle GMK = 90°$.

the first Brillouin zone edge, the calculation of which will be discussed later. In this paper, to further simplify the calculation of Eq. (4), we take the mean of the sine function and use the following formula to calculate v_p [48]:

$$E = 4.192 \times 10^{-4} v_p \times Q_{\max} \times \frac{\sqrt{2}}{2}. \qquad (5)$$

2. Length of first Brillouin zone edge

The basis vector of hexagonal lattice ($\overrightarrow{a_1}$, $\overrightarrow{a_2}$, and $\overrightarrow{a_3}$) can be expressed as

$$\overrightarrow{a_1} = \frac{\sqrt{3}a}{2}\overrightarrow{i} + \frac{a}{2}\overrightarrow{j}$$

$$\overrightarrow{a_2} = -\frac{\sqrt{3}b}{2}\overrightarrow{i} + \frac{b}{2}\overrightarrow{j}$$

$$\overrightarrow{a_3} = c\overrightarrow{k}, \qquad (6)$$

in which, a, b, and c are lattice parameters, and a is equal to b. According to the relation between real lattice and reciprocal lattice,

$$\overrightarrow{g_1} = 2\pi\frac{\overrightarrow{a_2} \times \overrightarrow{a_3}}{\Omega}, \qquad \overrightarrow{g_2} = 2\pi\frac{\overrightarrow{a_3} \times \overrightarrow{a_1}}{\Omega},$$

$$\overrightarrow{g_3} = 2\pi\frac{\overrightarrow{a_1} \times \overrightarrow{a_2}}{\Omega}. \qquad (7)$$

The basis vector of the reciprocal lattice ($\overrightarrow{g_1}$, $\overrightarrow{g_2}$, and $\overrightarrow{g_3}$) can be obtained:

$$\overrightarrow{g_1} = \frac{\sqrt{3}h}{2}\overrightarrow{i} + \frac{h}{2}\overrightarrow{j},$$

$$\overrightarrow{g_2} = -\frac{\sqrt{3}l}{2}\overrightarrow{i} + \frac{l}{2}\overrightarrow{j},$$

$$\overrightarrow{g_3} = m\overrightarrow{k}, \qquad (8)$$

where h, l, and m are reciprocal lattice parameters, in which h is equal to l. It can be seen from Fig. 1(b) that k point G to M is in the direction of reciprocal lattice vector $\overrightarrow{g_2}$, and combined with the geometric relationship in Fig. 1(c), the $Q_{\max}$ can be obtained according to the equations as follows:

$$Q_{GM} = l \quad Q_{KG} = \frac{2}{\sqrt{3}}l. \qquad (9)$$

Based on the above calculation, the length of the Brillouin region boundary Q_{GM} and Q_{KG} can be obtained under pressure.
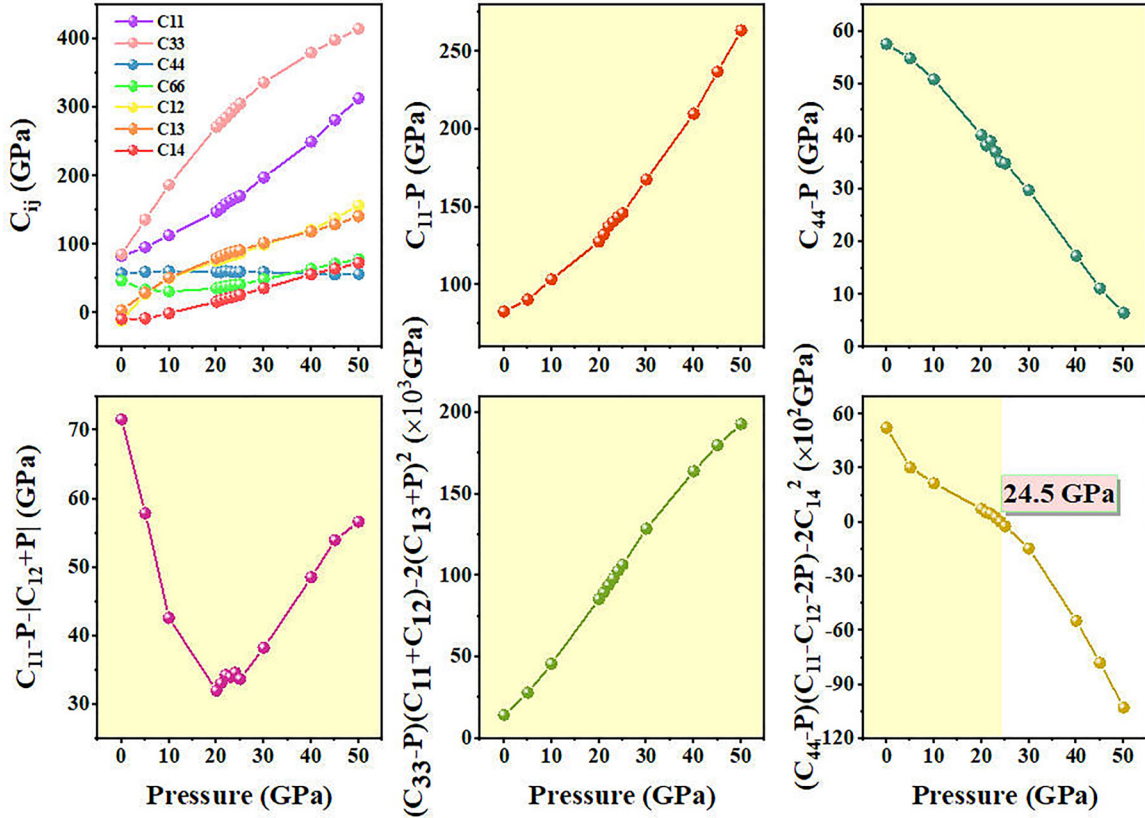
FIG. 2. The elastic properties of α-quartz: (a) the elastic constants under pressure, (b)–(f) the mechanical stability criterion of trigonal α-quartz under pressure.

B. Computational details

All calculations in this paper are adopted within CASTEP package based on the density functional theory (DFT) and the density functional perturbation theory (DFPT) [49]. The generalized gradient approximation (GGA) with Perdew-Burke-Ernzerhof (PBE) is performed to deal with exchange correlation effects [50,51]. The nonconserving pseudopotential is chosen to describe the interaction between electrons and ions, and [Si] $3s^2 3p^2$ and [O] $2s^2 2p^4$ electrons are constructed as valence electrons [52]. We use 5.0×10^{-6} eV/atom of energy, 0.01 eV/Å of maximum force, 0.02 GPa of maximum stress, and 5.0×10^{-4} Å of maximum displacement as the convergence tolerance to optimize the crystal structure. Moreover, the energy cutoff with 830 eV is selected to control the number of plane wave basis functions [53]. The Brillouin zones are carried over the $3 \times 3 \times 4$ grid sizes according to the strength of the Monkhorst-Pack scheme in the reciprocal space [54]. The linear response method is used to calculate the phonon dispersion [55].

III. RESULTS AND DISCUSSION

A. Mechanical stability and dynamics stability

The elastic constants under pressure are shown in Fig. 2(a), and it can be found that C_{11}, C_{33}, C_{12}, C_{13}, and C_{14} increase under pressure, while C_{44} increases within 0–10 GPa, and then decreases under pressure. Moreover, C_{66} decreases within a pressure range approximately 0–10 GPa,

and then increases under pressure, and this trend had been reported previously [28]. Figures 2(b)–2(f) intuitively show the mechanical stability criterion of trigonal α-quartz under pressure (see SM Sec. I [37]), indicating that structural mechanics instability occurs at around 24.5 GPa, that is, $(C_{44} - P)(C_{11} - C_{12} - 2P) - 2C_{14}^2 < 0$ at 24.5 GPa. This is basically consistent with the pressure point (22.3 GPa) of mechanical instability in α-quartz obtained by the constant-pressure molecular dynamics calculations [27]. Nevertheless, the phonon dispersion curves under pressure indicates that the structure becomes dynamically unstable until about 40 GPa, as shown in Fig. 3. It can be drawn from Fig. 3 that the acoustic phonons in the b and c axes do not appear as imaginary frequency under pressure, while acoustic phonons in the a axis appear as imaginary frequency at 40 GPa, and the imaginary frequency phenomenon becomes increasingly severe under pressure. This reveals that the lattice vibration in the b- and c-axis direction is dynamically stable, while the lattice vibration in the a-axis direction is dynamically unstable after 40 GPa, which mainly occurs at the edge of the Brillouin zone K and M.

B. Sound velocities

Based on previous studies described in the Introduction, we speculate that the main reason why the mechanically instability of α-quartz precedes the dynamic instability under pressure is that the amorphization of α-quartz under pressure. In order to understand the changes in structure under pressure
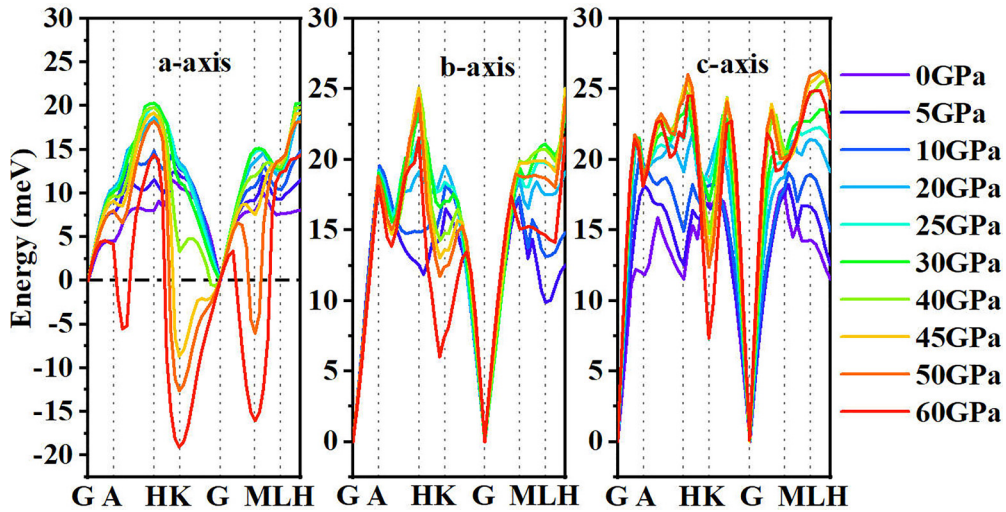
FIG. 3. The acoustic phonon dispersion curves of α-quartz in a, b, c axis under pressure.

after 24.5 GPa, we calculated the sound velocity.v_m, v_l, and v_t under pressure are displayed in Fig. 4, which signal that v_l increases under pressure, while v_t decreases under pressure. The former (v_l) is larger than the latter (v_t), and the difference between the two becomes larger under pressure. The decrease for v_t under pressure corresponds to an overall softening of acoustic phonon in the a and b axes, and the increase for v_l under pressure corresponds to an overall increase for acoustic phonon energy in the c axis. In addition, v_m decreases under pressure.

Further, the v_p and v_q along the directions of K to G and G to M in the a, b, and c axes can be obtained, as shown in Fig. 5. In the a axis [Fig. 5(a)], along the direction of K to G, v_p increases in the range 0–20 GPa, and then decreases in the range 20–40 GPa. Along the direction of G to M, v_p increases in the range 0–30 GPa, and then decreases in the range 30–48 GPa. Due to the appearance of an acoustic phonon with imaginary frequencies at the k points K at 40 GPa in the a axis, we deduce that beginning from 40 GPa the lattice vibration along
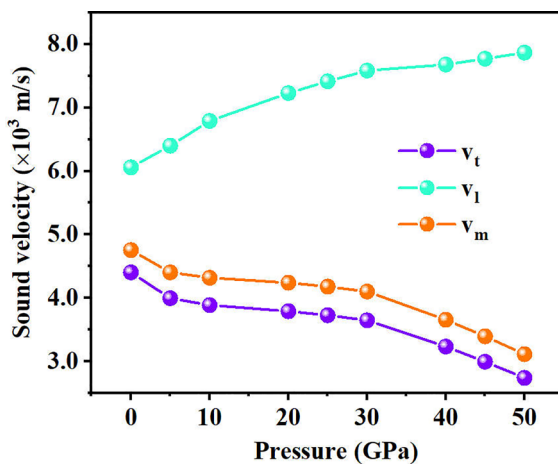
K to G in the a axis become propagated as plastic waves. For the same reason, starting from 48 GPa, lattice vibrations along the a axis from G to M become propagated as plastic waves. In this paper, v_q is used to describe the propagation speed of this plastic wave, and the results are plotted in Fig. 5(d). It can be seen that v_q increases under pressure, where v_q along the K to G direction is greater than v_q along the G to M direction, and the values of the two become closer under pressure. As can be seen from Fig. 5(b), in the b axis, along the K to G direction, v_p decreases from 0 to 5 GPa, increases from 5 to 20 GPa, and then decreases basically linearly from 20 to 60 GPa. Moreover, along the G to M direction, v_p increases from 0 to 5 GPa, decreases from 0 to 10 GPa, increases from 10 to 25 GPa, and then remains essentially constant, and decreases from 40 GPa. From Fig. 5(c), it can be seen that in the c axis, along the K to G direction, v_p decreases in the range 0–5 GPa, increases in the range 5–20 GPa, and gradually decreases in the range 20–60 GPa. Furthermore, along the G to M direction, v_p decreases in the range 0–10 GPa, remains basically unchanged in the range 10–20 GPa, increases in the range 20–30 GPa, and decreases in the range 30–60 GPa.

A comparative analysis of Figs. 5(a)–5(c) shows that v_p along the G to M direction is greater than v_p along the K to G direction regardless of the a, b, or c axis. Besides, it is found that v_p decreases after 20 GPa along the K to G direction and the decrease rate is faster, while along the G to M direction, v_p decreases after 30 GPa and the decrease rate is lower with the exception for the a axis. Moreover, we find a very interesting rule that the pressure point at which the v_p in any direction begins to decrease under pressure is between 20 and 25 GPa, which coincides with the pressure point (24.5 GPa) of the mechanical instability. Based on this, we suspect that the mechanical instability of 24.5 GPa is due to the amorphous nature of α-quartz, which is exactly consistent with the structure obtained by Tse *et al.* [27]. The dynamic instability of 40 GPa is due to structural changes under pressure, which is basically consistent with the conclusion drawn by Haines [1].
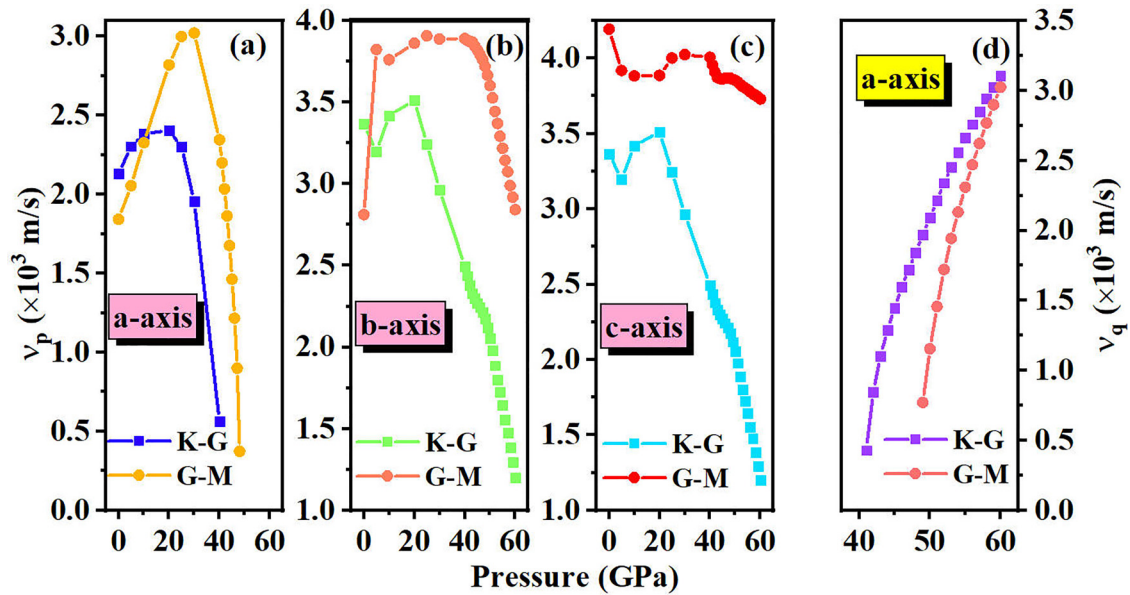

FIG. 4. The average sound velocity (v_m), the longitudinal (v_l) and transverse (v_t) wave sound velocity of α-quartz under pressure.

FIG. 5. The v_p along the direction of K to G and G to M in (a) a axis, (b) b axis, (c) c axis, and (d) the v_q along K to G and G to M in a axis.

IV. CONCLUSION

In conclusion, this paper mainly discusses the stability of α-quartz by analyzing the sound velocity under pressure. The calculation results show that the α-quartz structure is mechanically and dynamically unstable near the pressure of 24.5 and 40 GPa, which is close to the pressure range 21–43 GPa for the amorphization and phase transition mentioned in the experiment [32]. In the a, b, and c axes, the compressional sound velocity along the direction of K to G decreases linearly after 20 GPa, and along the direction of G to M it decreases after 30 GPa with relatively slower speed. Consequently, we deduce that the structural change occurs first along the direction of K to G no matter whether in the a axis, b axis, or c axis, and it is shown that the K to G direction in the a axis is the first to undergo structural changes.

In addition, the propagation velocities of plastic waves are described after lattice vibrational dynamic instability along the directions of K to G and G to M in the a axis. However, due to the essential differences between the plastic wave and the elastic wave, this paper directly uses the solution of compressional sound velocity to describe the propagation velocity of the plastic wave with a lack of theoretical basis. In addition, whether the specific value of imaginary frequency of a phonon has a theoretical reference value is also worth discussing. We will further discuss this in our subsequent research. Nevertheless, it is worth affirming that there is a certain reference value for the direction of structural change of α-quartz under pressure.

The data that support the findings of this study are available from the corresponding author upon reasonable request.

[1] J. Haines, J. M. Léger, F. Gorelli, and M. Hanfland, Crystalline post-quartz phase in silica at high pressure, Phys. Rev. Lett. **87**, 155503 (2001).

[2] T. Tsuchiya, R. Caracas, and J. Tsuchiya, First principles determination of the phase boundaries of high-pressure polymorphs of silica, Geophys. Res. Lett. **31**, L11610 (2004).

[3] Y. Kuwayama, K. Hirose, N. Sata, and Y. Ohishi, The pyrite-type high-pressure form of silica, Science **309**, 923 (2005).

[4] K. P. Driver, R. E. Cohen, Z. G. Wu, B. Militzer, P. López Ríos, M. D. Towler, R. J. Needs, and J. W. Wilkins, Quantum monte carlo computations of phase stability, equations of state, and elasticity of high-pressure silica, Proc. Natl. Acad. Sci. USA **107**, 9519 (2010).

[5] M. Murakami, K. Hirose, S. Ono, and Y. Ohishi, Stability of $CaCl_2$-type and A-PbO_2-type SiO_2 at high pressure and temperature determined by in-situ X-ray measurements, Geophys. Res. Lett. **30**, 1207 (2003).

[6] Y. Tsuchida and T. Yagi, A new, post-stishovite high-pressure polymorph of silica, Nature (London) **340**, 217 (1989).

[7] K. J. Kingma, R. E. Cohen, R. J. Hemley, and H. K. Mao, Transformation of stishovite to a denser phase at lower-mantle pressures, Nature (London) **374**, 243 (1995).

[8] L. S. Dubrovinsky, S. K. Saxena, P. Lazor, R. Ahuja, O. Eriksson, J. M. Wills, and B. Johansson, Experimental and theoretical identification of a new high-pressure phase of silica, Nature (London) **388**, 362 (1997).

[9] B. B. Karki, M. C. Warren, L. Stixrude, G. J. Ackland, and J. Crain, *Ab initio* studies of high-pressure structural transformations in silica, Phys. Rev. B **55**, 3465 (1997).

[10] D. M. Teter, R. J. Hemley, G. Kresse, and J. Hafner, High pressure polymorphism in silica, Phys. Rev. Lett. **80**, 2145 (1998).

[11] F. T. Mackenzie and R. Gees. Quartz: Synthesis at earth-surface conditions, Science **173**, 533 (1971).

[12] A. J. Leadbetter, T. W. Smith, and A. F. Wright, Structure of high cristobalite, Nat. Phys. Sci. **244**, 125 (1973).

[13] J. A. Klasik, High cristobalite and high tridymite in a middle eocene deep-sea chert, Science **189**, 631 (1975).

[14] E. C. T. Chao, E. M. Shoemaker, and B. M. Madsen, First natural occurrence of coesite, Science **132**, 220 (1960).

[15] D. D. Klug, R. Rousseau, K. Uehara, M. Bernasconi, Y. Le Page, and J. S. Tse, *Ab initio* molecular dynamics study of the pressure-induced phase transformations in cristobalite, Phys. Rev. B **63**, 104106 (2001).

[16] N. Y. Sun, W. G. Shi, Z. Mao, C. J. Zhou, and V. B. Prakapenka, High pressure-temperature study on the thermal equations of state of seifertite and $CaCl_2$-type SiO_2, J. Geophys. Res.: Solid Earth **124**, 12620 (2019).

[17] M. Miyahara, S. Kaneko, E. Ohtani, T. Sakai, T. Nagase, M. Kayama, H. Nishido, and N. Hirao, Discovery of seifertite in a shocked lunar meteorite, Nat. Commun. **4**, 1737 (2013).

[18] T. Tsuchiya and S. Nakagawa, A new high-pressure structure of SiO_2 directly converted from α-quartz under nonhydrostatic compression, J. Phys.: Condens. Matter **34**, 304003 (2022).

[19] S. Tsuneyuki, Y. Matsui, H. Aoki, and M. Tsukada, New pressure-induced structural transformations in silica obtained by computer simulation, Nature (London) **339**, 209 (1989).

[20] Y. Tsuchida and T. Yagi, New pressure-induced transformation of silica at room temperature, Nature (London) **347**, 267 (1990).

[21] D. C. Palmer, R. J. Hemley, and C. T. Prewitt, Raman spectroscopic study of high-pressure phase transitions in cristobalite, Phys. Chem. Miner. **21**, 481 (1994).

[22] R. T. Downs and D. C. Palmer, The pressure behavior of α-cristobalite, Am. Mineral. **79**, 9 (1994).

[23] A. Onodera, K. Suito, J. Namba, Y. Taniguchi, T. Horikawa, M. Miyoshi, O. Shimomura, and T. Kikegawa, Synchrotron x-ray-diffraction study of α-cristobalite at high pressure and high temperature, Int. J. High Pressure Res. **15**, 307 (1997).

[24] P. Dera, J. D. Lazarz, V. B. Prakapenka, M. Barkley, and R. T. Downs, New insights into the high-pressure polymorphism of SiO_2 cristobalite, Phys. Chem. Miner. **38**, 517 (2011).

[25] A. Černok, K. Marquardt, R. Caracas, E. Bykova, G. Habler, H. P. Liermann, M. Hanfland, M. Mezouar, E. Bobocioiu, and L. Dubrovinsky, Compressional pathways of a-cristobalite, structure of cristobalite X-I, and towards the understanding of seifertite formation, Nat. Commun. **8**, 15647 (2017).

[26] R. J. Hemley, A. P. Jephcoat, H. K. Mao, L. C. Ming, and M. H. Manghnan, Pressure-induced amorphization of crystalline silica, Nature (London) **334**, 52 (1988).

[27] J. S. Tse and D. D. Klug, Mechanical instability of a-quartz: A molecular-dynamics study, Phys. Rev. Lett. **67**, 3559 (1991).

[28] N. Binggeli and J. R. Chelikowsky, Elastic instability in α-quartz under pressure, Phys. Rev. Lett. **69**, 2220 (1992).

[29] K. J. Kingma, C. Meade, R. J. Hemley, H. K. Mao, and D. R. Veblen, Microstructural observations of α-quartz amorphization, Science **259**, 666 (1993).

[30] K. J. Kingma, R. J. Hemley, H. K. Mao, and D. R. Veblen, New high-pressure transformation in α-quartz, Phys. Rev. Lett. **70**, 3927 (1993).

[31] N. Binggeli, J. R. Chelikowsky, and R. M. Wentzcovitch, Simulating the amorphization of α-quartz under pressure, Phys. Rev. B **49**, 9336 (1994).

[32] K. J. Kingma, H. K. Mao, and R. J. Hemley, Synchrotron X-ray diffraction of SiO_2 to multimegabar pressures, High Pressure Res. **14**, 363 (1996).

[33] J. S. Tse, D. D. Klug, Y. L. Page, and M. Bernasconi, High-pressure four-coordinated structure of SiO_2, Phys. Rev. B **56**, 10878 (1997).

[34] X. D. Zhang and W. Jiang, First-principles investigation on vibrational, anisotropic elastic and thermodynamic properties for $L1_2$ structure of Al_3Er and Al_3Yb under high pressure, Philos. Mag. **96**, 320 (2016).

[35] Y. O. Ciftci, M. Evecen, and İ. O. Alp, Pressure effects on electronic, elastic, and vibration properties of metallic antiperovskite $PbNCa_3$ by ab initio calculations, J. Mol. Model. **27**, 7 (2021).

[36] J. Yang, J. H. Huang, Z. Yea, D. Y. Fan, S. H. Chen, and Y. Zhao, First-principles calculations on structural energetics of Cu-Ti binary system intermetallic compounds in Ag-Cu-Ti and Cu-Ni-Ti active filler metals, Ceram. Int. **43**, 7751 (2017).

[37] See Supplemental Material at http://link.aps.org/supplemental/10.1103/PhysRevB.109.144105 for further details about the structural properties, electronic properties, and elastic modulus of α-quartz under pressure, which includes Refs. [4,27,36,38–46].

[38] W. G. Li, Y. D. Gan, Z. X. Bai, X. H. Li, F. S. Liu, Z. T. Liu, Q. J. Liu, D. Hong, and X. H. Chang, The effect of pressure on the structural, electronic and vibrational properties of solid carbon dioxide phases, Phys. Chem. Chem. Phys. **24**, 4462 (2022).

[39] Y. S. Luo, Y. P. Cang, and D. Chen, Insights into elastic and thermodynamics properties of binary intermetallics in Ni-Al alloys under extreme condition: Full-electronic quasi-harmonic study, Chin. J. Chem. Phys. **27**, 399 (2014).

[40] J. Gao, Q. J. Liu, and B. Tang, Elastic stability criteria of seven crystal systems and their application under pressure: Taking carbon as an example, J. Appl. Phys. **133**, 135901 (2023).

[41] W. Voigt, *Lehrbuch der Kristallphysik* (Teubner, Leipzig, 1928).

[42] A. Reuss, Berechnung der Fließgrenze von Mischkristallen auf Grund der Plastizitätsbedingung für Einkristalle, Z. Angew. Math. Mech. **9**, 49 (1929).

[43] R. Hill, The elastic behaviour of a crystalline aggregate, Proc. Phys. Soc. **65**, 349 (1952).

[44] J. Glinnemann, H. E. King, H. Schulz, Th. Hahn, S. J. La Placa, and F. Dacol, Crystal structures of the low-temperature quartz-type phases of SiO_2 and GeO_2 at elevated pressure, Z. Kristallogr. - Cryst. Mater. **198**, 177 (1992).

[45] C. G. Wu, W. Y. Wu, Y. C. Gong, B. F. Dai, S. H. He, and Y. H. Huang, First-principles study on the band-gap changes of Zn_2GeO_4 under high pressure, Acta Phys. Sin. **64**, 114213 (2015).

[46] Y. Deng, R. Z. Wang, L. C. Xu, H. Fang, and H. Yan, Pressure induced band-gap changes in $(Ba_{0.5}Sr_{0.5})TiO_3$ (BST) from first-principles calculations, Acta Phys. Sin. **60**, 117309 (2011).

[47] T. Sakamaki, E. Ohtani, H. Fukui, S. Kamada, S. Takahashi, T. Sakairi, A. Takahata, T. Sakai, S. Tsutsui, D. Ishikawa, R. Shiraishi, Y. Seto, T. Tsuchiya, and A. Q. R. Baron, Constraints

on Earth's inner core composition inferred from measurements of the sound velocity of hcp-iron in extreme conditions, Sci. Adv. **2**, e1500802 (2016).

[48] C. L. Jiang, W. Zeng, Y. D. Gan, F. S. Liu, B. Tang, and Q. J. Liu, Structural softening of solid nitrogen under pressure by first-principles calculations, J. Phys. Chem. Solids **146**, 109616 (2020).

[49] S. J. Clark, M. D. Segall, C. J. Pickard, P. J. Hasnip, M. I. J. Probert, K. Refson, and M. C. Payne, First principles methods using CASTEP, Z. Kristallogr. - Cryst. Mater. **220**, 567 (2005).

[50] J. P. Perdew, K. Burke, and M. Ernzerhof, Generalized gradient approximation made simple, Phys. Rev. Lett. **77**, 3865 (1996).

[51] J. P. Perdew, A. Ruzsinszky, G. I. Csonka, O. A. Vydrov, G. E. Scuseria, L. A. Constantin, X. L. Zhou, and K. Burke, Restoring the density-gradient expansion for exchange in solids and surfaces, Phys. Rev. Lett. **100**, 136406 (2008).

[52] D. Vanderbilt, Soft self-consistent pseudopotentials in a generalized eigenvalue formalism, Phys. Rev. B **41**, 7892 (1990).

[53] B. G. Pfrommer, M. Côté, S. G. Louie, and M. L. Cohen, Relaxation of crystals with the quasi-newton method, J. Comput. Phys. **131**, 233 (1997).

[54] H. J. Monkhorst and J. D. Pack, Special points for Brillouin-zone integrations, Phys. Rev. B **13**, 5188 (1976).

[55] S. Baroni, S. de Gironcoli, A. D. Corso, and P. Giannozzi, Phonons and related crystal properties from density-functional perturbation theory, Rev. Mod. Phys. **73**, 515 (2001).